npj | antimicrobials and resistance

www.nature.com/npjamar

ARTICLE OPEN

Check for updates

Loss of allosteric regulation in α-isopropylmalate synthase identified as an antimicrobial resistance mechanism

Jaryd R. Sullivan[1,2,3], Christophe Courtine[1,2,6], Lorne Taylor[4], Ori Solomon[1,2,3] and Marcel A. Behr[1,2,3,5]✉

Despite our best efforts to discover new antimicrobials, bacteria have evolved mechanisms to become resistant. Resistance to antimicrobials can be attributed to innate, inducible, and acquired mechanisms. *Mycobacterium abscessus* is one of the most antimicrobial resistant bacteria and is known to cause chronic pulmonary infections within the cystic fibrosis community. Previously, we identified epetraborole as an inhibitor against *M. abscessus* with in vitro and in vivo activities and that the efficacy of epetraborole could be improved with the combination of the non-proteinogenic amino acid norvaline. Norvaline demonstrated activity against the *M. abscessus* epetraborole resistant mutants thus, limiting resistance to epetraborole in wild-type populations. Here we show *M. abscessus* mutants with resistance to epetraborole can acquire resistance to norvaline in a leucyl-tRNA synthetase (LeuRS) editing-independent manner. After showing that the membrane hydrophobicity and efflux activity are not linked to norvaline resistance, whole-genome sequencing identified a mutation in the allosteric regulatory domain of α-isopropylmalate synthase (α-IPMS). We found that mutants with the α-IPMS^{A555V} variant incorporated less norvaline in the proteome and produced more leucine than the parental strain. Furthermore, we found that leucine can rescue growth inhibition from norvaline challenge in the parental strain. Our results demonstrate that *M. abscessus* can modulate its metabolism through mutations in an allosteric regulatory site to upregulate the biosynthesis of the natural LeuRS substrate and outcompete norvaline. These findings emphasize the antimicrobial resistant nature of *M. abscessus* and describe a unique mechanism of substrate-inhibitor competition.

npj Antimicrobials & Resistance (2023)1:7 ; https://doi.org/10.1038/s44259-023-00005-4

INTRODUCTION

Antimicrobial resistance (AMR) is a major public health concern and is estimated to contribute to 5 million deaths each year[1–3]. To facilitate antimicrobial research and development, the WHO created a priority pathogen list based on trends of resistance, preventability, and the status of the drug pipeline[4,5]. Pathogens on this list are considered critical, high, or medium priority with a separate designation for *Mycobacterium tuberculosis*. Arguably, when compared to *M. tuberculosis*, *M. abscessus* is more drug resistant, more recalcitrant to treatment, and has less lead compounds in its pipeline than *M. tuberculosis*, yet it is often neglected in discussions regarding the current threat of antimicrobial-resistant bacteria[6–10].

Resistance to antimicrobials can be attributed to innate, inducible, and acquired mechanisms. *M. abscessus* uses a variety of mechanisms to overcome the antibiotic regimens clinicians have at their disposal. Besides acquired target mutations that alter the binding affinity for antibiotics like clarithromycin[11], *M. abscessus* has a complex phenotypic resistome. The *M. abscessus/M. chelonae* complex is recognized for its unusually hydrophobic membrane relative to *M. tuberculosis*, which decreases the permeability to small nutrients and amino acids, and antibiotics across the cell wall[12,13]. Moreover, it has also been established that the cell wall synergizes with the internal resistome that includes efflux pumps and drug modifying enzymes to limit the effect of toxic compounds[6]. *M. abscessus* expresses the ADP-ribosyltransferase arr_{Mab} that ribosylates rifamycins, and the *N*-acetyltransferase *eis2* and 3′-*O*-phosphotransferase *aph(3′)* that inactivate aminoglycosides[14–17]. The genome also encodes the β-lactamases Bla_{Mab}, which can hydrolyze penicillins and cephalosporins, and Bla_{Mmas}, which has extended spectrum activity against carbapenems to limit the availability of the most widely-used antibiotic class used to treat bacterial infections[18–20]. Many of the mechanisms listed here are under the regulation of inducible transcription factors like WhiB7. WhiB7 is known to be activated by ribosomal protein synthesis inhibitors like macrolides, tetracyclines, and aminoglycosides but also by molecules with pleiotropic effects on cell metabolism[21–23]. It was shown in *M. abscessus* that inducible macrolide resistance is mediated through upregulation of *erm*(41) in a WhiB7-dependent process[24–26]. These mechanisms act in synergy with a hydrophobic membrane composed of mycolic acids with significantly less permeability than the membranes of other mycobacteria, resulting a majority of treatment failures[12,13,27,28].

By elucidating AMR mechanisms and leveraging the bacterial response to antimicrobial agents, novel antimicrobials and combination therapies could be developed for *M. abscessus* infections. Previously, we identified the leucyl-tRNA synthetase (LeuRS) inhibitor epetraborole with nanomolar whole-cell activity against *M. abscessus*[29]. During this screening programme, we discovered that epetraborole had failed a phase 2 clinical trial due to the rapid emergence of resistant *Escherichia coli* in complicated urinary tract infections[30]. We showed that epetraborole resistant *M. abscessus* mutants became sensitive to the non-proteinogenic amino acid L-norvaline.

[1]Infectious Diseases and Immunity in Global Health Program, Research Institute of the McGill University Health Centre, Montreal, QC H4A 3J1, Canada. [2]Department of Microbiology & Immunology, McGill University, Montreal, QC H3A 2B4, Canada. [3]McGill International TB Centre, Montreal, QC H4A 3S5, Canada. [4]Clinical Proteomics Platform, Research Institute of the McGill University Health Centre, Montreal, QC H4A 3J1, Canada. [5]Department of Medicine, McGill University Health Centre, Montreal, QC H3G 2M1, Canada. [6]Present address: Department of Microbiology and Immunology, Geisel School of Medicine at Dartmouth College, Hanover, NH 03755, USA.
✉email: marcel.behr@mcgill.ca

L-Norvaline is an uncommon amino acid with limited examples found in nature or laboratory conditions. L-Norvaline has been identified in an antifungal peptide produced by *Bacillus subtilis*, and leucine biosynthesis regulatory mutants of *Serratia marcescens*[31,32]. Recombinant protein production in *E. coli* can result in trace amounts of norvaline incorporation in leucine-rich proteins and micro-aerophilic growth conditions can stimulate norvaline production[33,34]. The absence of L-norvaline in nature suggests its role in biology has been supplanted by alternative amino acids. Indeed, it has been hypothesized that norvaline is a relic from the early stages of evolution and was replaced by L-leucine[35]. Evidence of this is supported with the conserved editing domain on LeuRS that was shown to be paramount to prevent mischarging $tRNA^{Leu}$ with norvaline[36].

Sensitivity to L-norvaline is derived from a D436H substitution in the editing domain of LeuRS, which is the binding site for the epetraborole-$tRNA^{Leu}$ adduct. Other mutations leading to epetraborole resistance like Y421D, T322I, and T323P have been identified in the editing domain of LeuRS but whether these mutants are susceptible to L-norvaline remains to be determined[29,37]. LeuRS activates L-leucine and subsequently transfers the activated amino acid onto the corresponding $tRNA^{Leu}$ isoacceptors. Fortunately, $tRNA^{Leu}$ with non-cognate amino acids can undergo hydrolysis in the editing domain to remove the erroneous amino acid before participating in polypeptide synthesis. However, by gaining resistance to epetraborole from $LeuRS^{D436H}$, the ability to edit misaminoacylated $tRNA^{Leu}$ is lost and the risk of translating incorrect proteins increases. Treatment of the epetraborole resistant mutants with L-norvaline caused proteome-wide misincorporation with L-norvaline at residues coding for L-leucine, and a decrease in the emergence of resistance to epetraborole when given in combination[29].

In this article, we show using a combination of genetics, proteomics, and small molecule analysis that overproduction of L-leucine from insensitivity to feedback inhibition can abrogate the toxicity of L-norvaline to levels similar to using the evolutionarily conserved editing domain on LeuRS. These findings demonstrate the loss of allosteric regulation as the foundation for competitive antimicrobial inhibition and highlight the propensity of *M. abscessus* to become increasingly antimicrobial resistant.

RESULTS

Spontaneous generation of L-norvaline resistance in *M. abscessus*

M. abscessus that is resistant to both epetraborole and L-norvaline was raised spontaneously during a kill kinetics experiment that sought to determine whether L-norvaline caused cell death to the epetraborole-resistant *M. abscessus* $LeuRS^{D436H}$ strain. The wild type ATCC 19977 reference strain of *M. abscessus*, the EPT^R D436H mutant, and the EPT^R D436H mutant complemented with wild type *leuS* were grown in 2.4 mM L-norvaline (4×MIC_{90}) for 5 days. In agreement with the editing activity of LeuRS, the wild type and complemented strains grew in 2.4 mM L-norvaline, unlike the editing-deficient mutant (Fig. 1a). For the latter strain, L-norvaline challenge resulted in a loss of viable bacteria, congruent with the toxicity from misfolded proteins. Unexpectedly, the growth of EPT^R D436H mutant recovered at later timepoints. We hypothesized that L-norvaline might degrade over time and repeated the experiment where 2.4 mM L-norvaline was supplemented each day to create a steady-state (4×SS). Again, however, the EPT^R D436H mutant grew after day 3 (Fig. 1a). To confirm resistance to L-norvaline, aliquots of the EPT^R D436H mutant grown without L-norvaline and in 4×SS were taken to measure the MIC_{90} of L-norvaline using the resazurin microtiter assay (REMA) method. Indeed, the EPT^R D436H 4XSS strain had a $MIC_{90} > 40$ mM while the original EPT^R D436H strain grown without L-norvaline had a MIC_{90} of 0.2 mM.

Since *M. abscessus* was shown to have inducible resistance to macrolides[26,38], we asked whether L-norvaline resistance was inducible or acquired. We previously showed that inducible macrolide resistance in *M. abscessus* can be repressed after passaging the culture in drug-free media for six days[29]. Aliquots of the EPT^R D436H strain grown in L-norvaline-free or 4XSS conditions on day five were passaged for 6 days in L-norvaline-free media. The MIC_{90} to L-norvaline, epetraborole, and amikacin were determined using REMA. We showed that L-norvaline resistance is not inducible since passaging the culture in L-norvaline-free media did not change the MIC_{90} (Fig. 1a). Alternatively, L-norvaline resistance could arise from a $LeuRS^{D436H}$ reversion where the population regains editing activity but becomes susceptible to epetraborole. Refuting this possibility, resistance to epetraborole was retained with $MIC_{90} > 0.05$ mM (Fig. 1a). Lastly, L-norvaline resistance was not the result of cross-resistance as evidenced with sensitivity to the control drug amikacin.

To further characterize the new mutant resistant to both epetraborole and L-norvaline, we challenged *M. abscessus* ATCC 19977, *M. abscessus* EPT^R D436H, and *M. abscessus* EPT^R Nva^R 4×SS with 0.5 mM L-norvaline and other branched-chain amino acids (BCAAs) in Sauton's minimal media and fit their growth to an exponential plateau regression (Fig. 1b). As controls, *M. abscessus* ATCC 19977 grew in L-norvaline while *M. abscessus* EPT^R D436H failed to grow. Like the ATCC 19977 reference strain, the growth of *M. abscessus* EPT^R Nva^R 4×SS was not impeded by 0.5 mM L-norvaline. From the exponential fit, we extracted the maximum growth plateau (Y_M) and growth rate (μ). Quantitatively, we observed that L-norvaline impairs both the maximum growth and growth rate of an editing deficient strain like *M. abscessus* EPT^R D436H but that *M. abscessus* EPT^R Nva^R 4×SS regained a normal growth rate with a lower plateau (Fig. 1c). Similar results were obtained when the experiments were repeated in nutrient rich 7H9 media (Supplementary Fig. 1).

Growth in 0.5 mM BCAAs was repeated on solid media using 7H10 base and 100 µM amikacin as control. We observed similar results where only *M. abscessus* EPT^R D436H failed to grow on 0.5 mM L-norvaline while amikacin inhibited all strains (Fig. 1d). These results (i) confirmed L-norvaline resistance and (ii) suggested an alternative mechanism of L-norvaline resistance acquired by *M. abscessus* that is editing independent.

Membrane hydrophobicity does not drive norvaline resistance

To examine whether the *M. abscessus* EPT^R Nva^R 4×SS mutant has a modified cell envelope, we measured the hydrophobicity via the uptake of Congo red dye. Strains were streaked onto 7H10 plates with 10% (v/v) OADC and 140 µM Congo red and incubated at 37 °C for 5 days (Fig. 2a). *M. abscessus* ATCC 19977 strains with the smooth morphotype (S) or rough morphotype (R) were used as representative hydrophilic and hydrophobic membranes, respectively. The rough morphotype contains a mutation in *mmpL4b*, which prevents the transport of glycopeptidolipids across the membrane and creates a uniform hydrophobicity across the cell envelope unlike the smooth morphotype that has clusters of hydrophobic domains[39]. This distribution of hydrophobic domains could play a role in limiting the uptake of L-norvaline. Gross visualization of the colonies indicated that both the parental EPT^R D436H and EPT^R Nva^R 4×SS strains had a smooth morphotype which favours pink colonies with red borders while the rough morphotype colonies were uniformly red (Fig. 2a). Congo red dye retained in the membrane was extracted with DMSO and quantified at 488 nm. We observed a significant increase in retained Congo red dye in *M. abscessus* R compared to S, however there was no significant change in dye retained in EPT^R Nva^R 4×SS

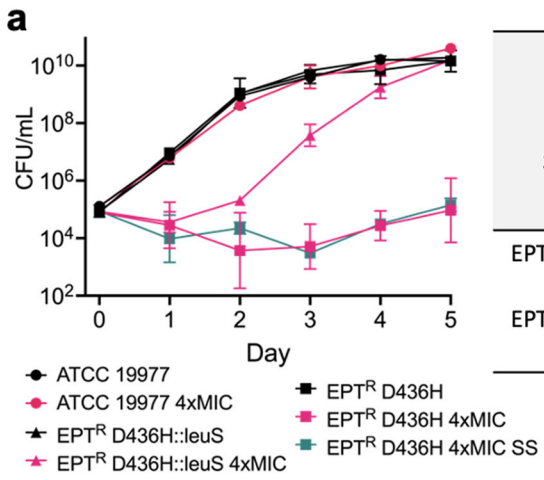

Strain	MIC_{90}			
	Day 5	+6 days passage		
	Nva (mM)	Nva (mM)	EPT (μM)	AMK (μM)
EPT^R D436H	0.2	0.2	>50	14
EPT^R D436H 4xSS	>40	>40	>50	15

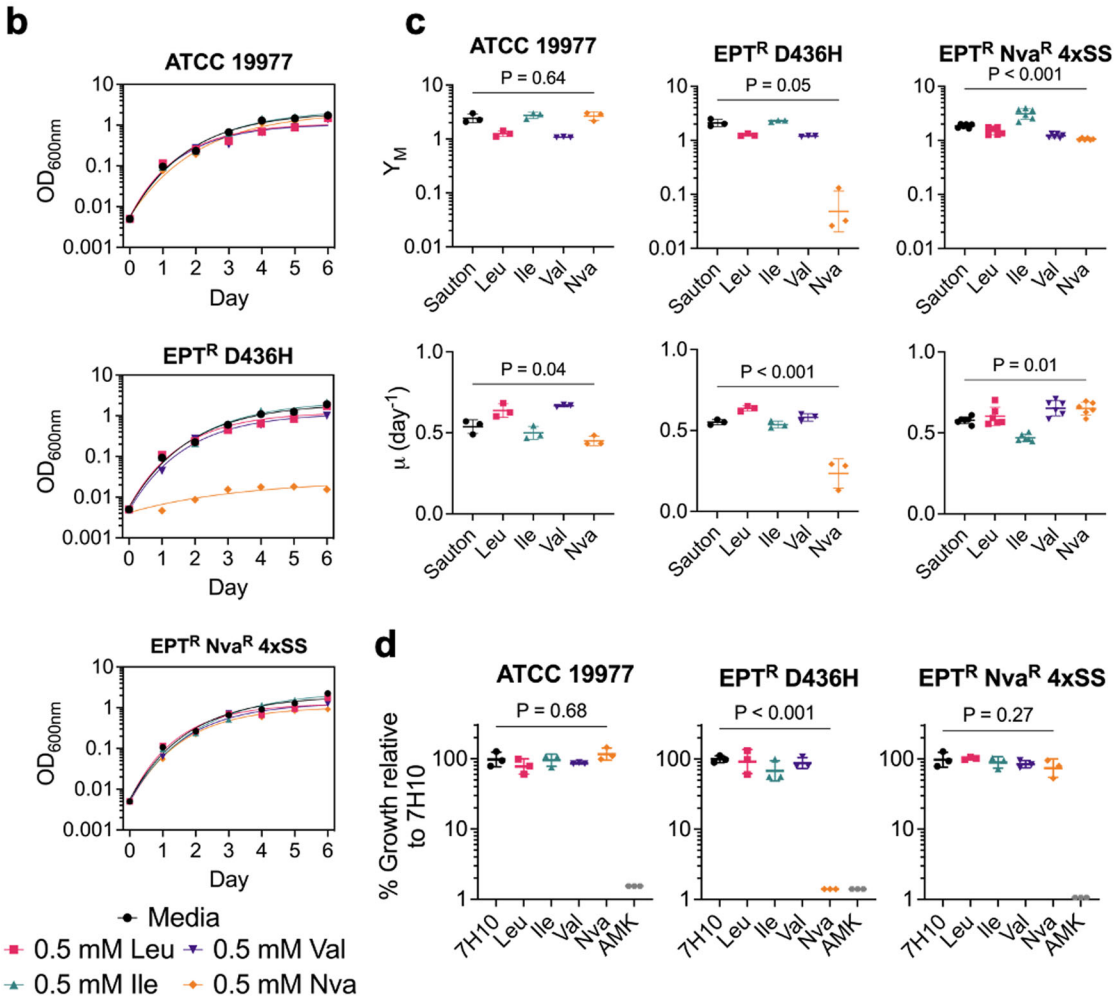

relative to the parental strain EPT^R D436H (Fig. 2b). These results suggest that the cell membrane of *M. abscessus* EPT^R Nva^R 4×SS has not undergone modifications to decrease the permeability to L-norvaline.

L-norvaline resistance is not mediated by efflux pump activity

Besides being involved in the architecture of the cell envelope some MmpL proteins have been shown to be antimycobacterial drug efflux pumps[40,41]. Most notably, this was demonstrated for the recently approved drug bedaquiline[42,43]. We speculated that the large number of efflux pumps in *M. abscessus* might contribute to L-norvaline resistance. To measure the net influx/efflux activity, we used an ethidium bromide (EtBr) accumulation assay previously used in *M. abscessus* and *M. tuberculosis* to assess drug resistance[44,45]. Initially, EtBr has limited fluorescence in aqueous solution but becomes appreciably fluorescent when intercalated with dsDNA[46]. The fluorescence (Ex/Em 525/600) of EtBr was measured over 2 h in wild-type *M. abscessus* incubated with serial dilutions of EtBr (Fig. 3a). Fluorescence time curves were fitted to

Fig. 1 Editing-deficient norvaline resistance in *M. abscessus*. **a** Left, WT *M. abscessus* ATCC 19977, *M. abscessus* EPT^R D436H, and *M. abscessus* EPT^R D436H complemented with WT LeuRS were grown in media free of exogenous L-norvaline or at 4×MIC$_{90}$ (MIC$_{90}$ = 0.6 mM) of the Nva^S/EPT^R *M. abscessus* D436H strain. Alternatively, *M. abscessus* EPT^R D436H strains were grown in media with an initial inoculum of 4×MIC$_{90}$, or media replenished with 4×MIC$_{90}$ daily to establish a steady-state of L-norvaline (SS). Data represents mean ± SD from $n = 2$–5 independent experiments. Right, Aliquots of *M. abscessus* EPT^R D436H grown in L-norvaline free media (black squares) or L-norvaline at 4×SS (teal squares) from day 5 were used to determine the MIC$_{90}$ of L-norvaline. Cultures were passaged for 6 days in L-norvaline free media before measuring the MIC$_{90}$ for L-norvaline, and control drugs epetraborole and amikacin. **b** Growth curves of *M. abscessus* ATCC 19977, *M. abscessus* EPT^R D436H, and mutant with dual EPT^R and Nva^R resistance raised at 4×SS. Strains were grown statically in 96-well plates with nutrient limited Sauton media ± BCAAs and fit with exponential plateau regression. Data are representative of n = 3 independent experiments with mean ± SD. *P* values were obtained by one-way ANOVA with Dunnett's multiple comparisons test. **c** Comparison of maximum growth plateau (Y_M) and growth rates (μ) in Sauton media ± BCAAs. Data is mean ± SD from $n = 3$ independent replicates with *M. abscessus* EPT^R Nva^R 4×SS in biological **d**uplicates. **d** Growth on solid 7H10 media ± BCAAs. 100 μM amikacin was used as control. Data are mean ± SD from $n = 3$ independent experiments. *P* values were obtained by one-way ANOVA with Dunnett's multiple comparisons test.

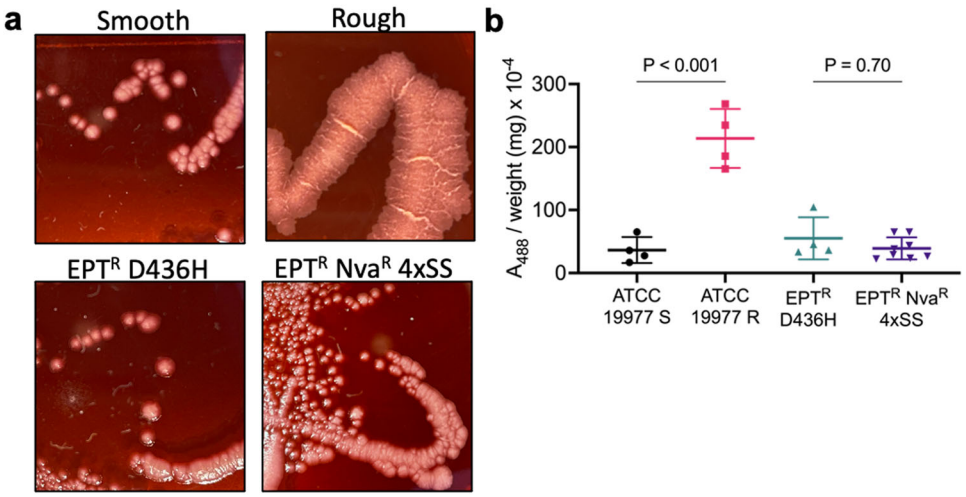

Fig. 2 Membrane hydrophobicity of *M. abscessus*. **a** Colony morphology of ATCC 19977-S (smooth), ATCC 19977-R (rough), *M. abscessus* EPT^R D436H, and *M. abscessus* EPT^R Nva^R 4×SS on 7H10 plates supplemented with 10% (v/v) OADC and Congo red at 140 μM. **b** Quantitative analysis of extracted Congo red dye retained in the membrane at A$_{488nm}$. Data represent mean ± SD of $n = 4$ independent experiments with *M. abscessus* EPT^R Nva^R 4×SS in biological duplicates. *P* values were obtained by one-way ANOVA with Tukey's multiple comparisons test.

an exponential plateau regression to determine the fluorescence at equilibrium (F_{eq}) and generate a dose–response curve (Fig. 3a inset). The fluorescence of intracellular EtBr was measured in wild type, EPT^{R}D436H, and EPT^R Nva^R 4×SS strains of *M. abscessus* at 6.25 μM EtBr. ATCC 19977 S and R morphotypes were used as controls. MmpL4b is non-functional in the rough morphotype, which either resulted in impaired efflux or increased permeability and thus, greater accumulation of EtBr (Fig. 3b). Although we measured a statistically significant difference in EtBr accumulation in the S morphotype compared to the R morphotype, the difference in F_{eq} between EPT^R Nva^R 4×SS and the parental strain EPT^R D436H was not statistically significant (Fig. 3b).

Next, we repeated the EtBr accumulation assay with verapamil and CCCP as efflux pump inhibitors[47]. Using 0.5 mM verapamil and 25 μM CCCP, we measured a statistically significant increase in the F_{eq} for all strains except *M. abscessus* R with CCCP (Fig. 3b, c). With the efflux pump inhibitors validated, we sought to determine the effect size ($\Delta F_{eq} = F_{drug} - F_{drug\ free}$) of verapamil and CCCP on efflux pump inhibition. Verapamil and CCCP had similar effect sizes against EPT^R Nva^R 4×SS and the parental strain EPT^R D436H, which suggests that the EPT^R Nva^R 4×SS strain does not have increased efflux activity (Fig. 3d).

α-IPMS^{A555V} variant participates in L-norvaline resistance

To identify the putative mutation(s) underlying L-norvaline resistance, gDNA was extracted from *M. abscessus* EPT^R D436H as the parental strain and two *M. abscessus* EPT^R Nva^R 4×SS mutants for whole-genome sequencing. All strains sequenced retained the C to G transversion at position 1306 in *leuS* that translates into LeuRS^{D436H}, which confirmed that resistance was not acquired through a D436H reversion as shown with the MIC to epetraborole (Fig. 1a). When compared to the parental strain, both EPT^R Nva^R 4×SS mutants sequenced had a unique C to T transition at position 1664 in *leuA* (*MAB_0337c*) which translates into LeuA^{A555V} and T to C transition at position 44 in tRNA$^{Leu(GAG)}$ (*MAB_t5031c*). *leuA* codes for α-isopropylmalate synthase (α-IPMS) which catalyses the carboxymethylation of 2-oxoisovalerate using acetyl-CoA to produce α-isopropylmalate as the first step in the L-leucine biosynthetic pathway. tRNA$^{Leu(GAG)}$ is one of the five encoded tRNA^{Leu} isoacceptors encoded in *M. abscessus*.

To determine which variant gene is responsible for the L-norvaline resistant phenotype, wild type and mutant *leuA* and tRNA$^{Leu(GAG)}$ were cloned with 250 bp upstream to capture the nascent promoter into the integrative vector pMV306. These constructs, as well as an empty pMV306 vector (EV) were electroporated into *M. abscessus* EPT^R D436H. Next, we measured the bacterial viability of *M. abscessus* ATCC 19977, parental *M. abscessus* EPT^R D436H, EPT^R D436H complemented with *leuA* or tRNA$^{Leu(GAG)}$, and the natural double mutant *M. abscessus* EPT^R Nva^R 4×SS against L-norvaline, epetraborole, and amikacin. Only *M. abscessus* EPT^R D436H complemented with the mutant *leuA* had increased resistance to L-norvaline; complementation with the wild type *leuA* had no effect (Supplementary Fig. 2a). All strains of *M. abscessus* with LeuRS^{D436H} retained resistance to epetraborole and all strains were equally susceptible to amikacin (Supplementary Fig. 2b, c). Increased viability to L-norvaline challenge was not observed when *M. abscessus* EPT^R D436H was

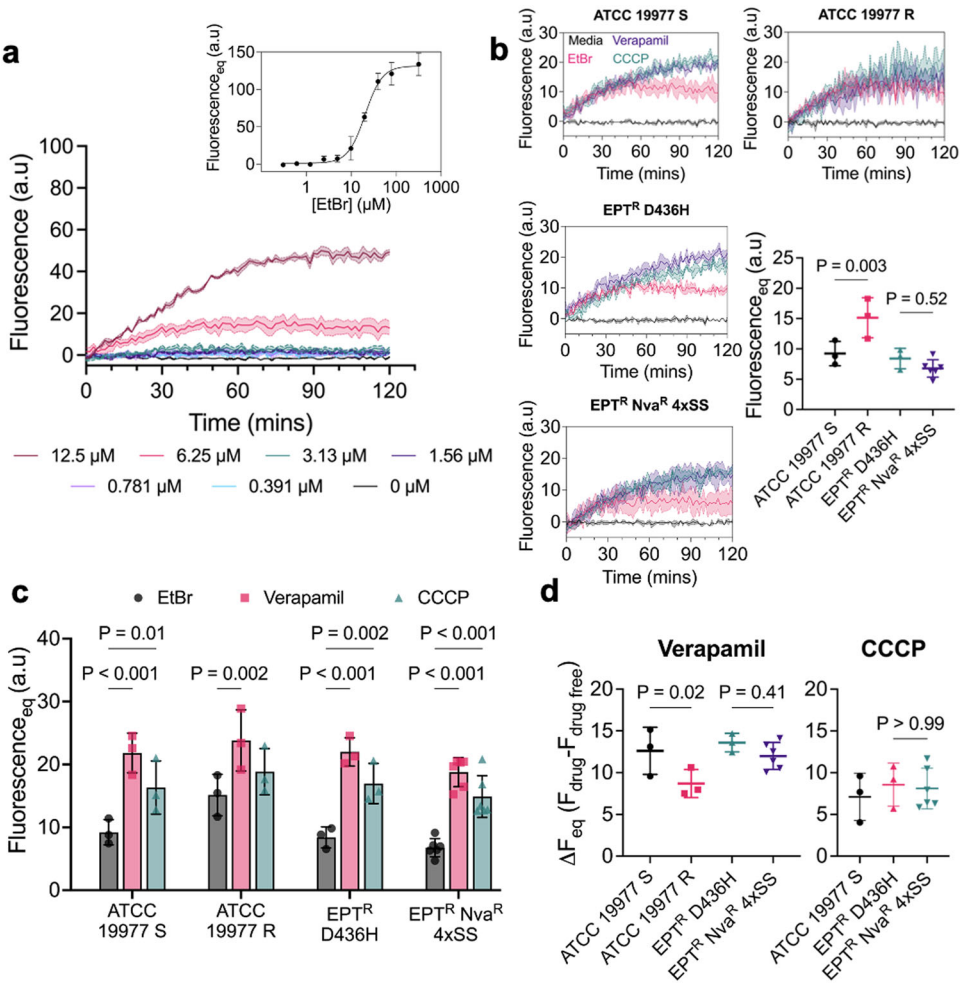

Fig. 3 Efflux activity of *M. abscessus*. **a** Dose–response curve of ethidium bromide (EtBr, Ex_{525nm}, Em_{600nm}) accumulation in *M. abscessus* ATCC 19977 S. **b** EtBr accumulation with 6.25 μM EtBr in ATCC 19977 S, ATCC 19977 R, *M. abscessus* EPT^R D436H, and *M. abscessus* EPT^R Nva^R 4×SS. 0.5 mM verapamil and 25 μM CCCP were used as efflux pump inhibitors in **b**. Data are mean ± SD of $n = 3$ independent replicates with *M. abscessus* EPT^R Nva^R 4×SS in biological duplicates. P values were obtained by one-way ANOVA with Sidak's multiple comparisons test. **c** Efflux pump inhibitors promote EtBr accumulation. Data are mean ± SD of $n = 3$ independent replicates with *M. abscessus* EPT^R Nva^R 4×SS in biological duplicates. *P* values were obtained by two-way ANOVA with Dunnett's multiple comparisons test. **d** Quantification of efflux pump inhibitor effect. ATCC 19977 R was omitted from CCCP as the effect was not statistically significant. Data is mean ± SD of $n = 3$ independent replicates with *M. abscessus* EPT^R Nva^R 4×SS in biological duplicates. *P* values were obtained by one-way ANOVA with Sidak's multiple comparisons test.

complemented with wild type or mutant *tRNA*$^{Leu(GAG)}$ (Supplementary Fig. 2d–f).

To corroborate the drug susceptibility results, we monitored the growth of *M. abscessus* ATCC 19977, *M. abscessus* EPT^R D436H, EPT^R D436H complemented with *leuA*, and *M. abscessus* EPT^R Nva^R 4×SS in Sauton's minimal media with 0.5 mM BCAAs. Complementing *M. abscessus* EPT^R D436H with the mutant variant of *leuA* nearly completely restored the growth in 0.5 mM L-norvaline relative to L-norvaline-free media while *M. abscessus* EPT^R D436H with wild-type *leuA* or the parental *M. abscessus* EPT^R D436H still exhibited reduced growth (Fig. 4a and Supplementary Fig. 3). These results suggest that α-IPMS^{A555V} alone is sufficient to impart the L-norvaline-resistant phenotype while the role of tRNA$^{Leu(GAG)T44C}$ is yet to be determined.

Previously, we showed that in the absence of LeuRS editing activity, L-norvaline is incorporated into proteins at sites coding for L-leucine[29]. Therefore, we hypothesized that the *M. abscessus* EPT^R Nva^R 4×SS mutant would lack high levels of norvalinated proteins after L-norvaline challenge. Cell lysates were collected from *M. abscessus* ATCC 19977, *M. abscessus* EPT^R D436H, complemented strains, and *M. abscessus* EPT^R Nva^R 4×SS after 24 h of growth in Sauton's minimal media with 0.5 mM L-norvaline and analysed by reverse-phase HPLC/MS. Principal component analysis (PCA) of cell lysate proteomes identified three proteomic clusters among the five strains with PC1 and PC2 accounting for 91% and 5% of variance, respectively (Fig. 4b and Supplementary Fig. 4a). Cluster 1 is the naturally L-norvaline resistant strain ATCC 19977, cluster 2 is the L-norvaline sensitive strain *M. abscessus* EPT^R D436H and its complement with wild type α-IPMS^{WT}, and cluster 3 is the editing independent L-norvaline resistant strain *M. abscessus* EPT^R Nva^R 4×SS and EPT^R D436H complemented with α-IPMS^{A555V}. The clusters were separated based on GroEL abundance in PC1 with a small contribution from Acyl-CoA dehydrogenase FadE abundance in PC2 (Fig. 4b and Supplementary Fig. 4b). Proteins with L-norvaline residues were identified by filtering for L-leucine residues missing the 14 Da methylene group absent on L-norvaline. As expected from the PCA results, *M. abscessus* ATCC 19977 maintained preferential incorporation of L-leucine

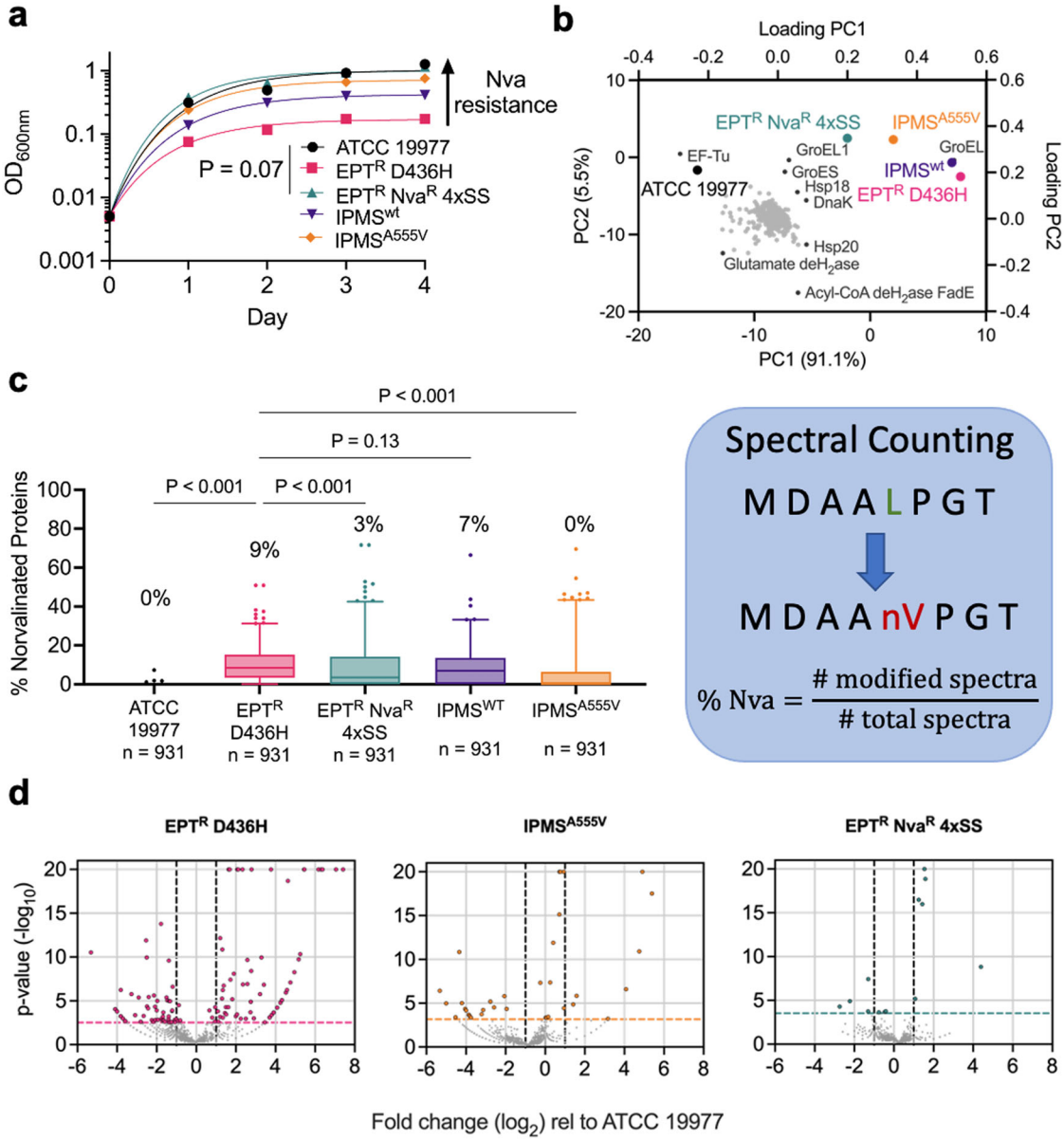

Fig. 4 ***M. abscessus*** **EPT^R Nva^R mutant uses alternative mechanism to limit L-norvaline toxicity. a** Reference strain ATCC 19977 (black circles), EPT^R D436H (pink squares), naturally raised EPT^R Nva^R 4×SS mutant (green triangles), EPT^R D436H mutant complemented with α-IPMS^{WT} (purple triangles) or α-IPMS^{A555V} (orange diamonds) grown in Sauton's minimal media with 0.5 mM L-norvaline and fit with exponential plateau regression. Data are representative of $n = 3$ independent experiments with mean ± SD of technical triplicates. *P* values were obtained by one-way ANOVA with Tukey's multiple comparisons test. **b** Principal component analysis of cell lysate proteomes after 24 h of growth in Sauton's media with 0.5 mM L-norvaline. PC1 accounted for 90% of the variance, PC2 accounted for 5% of the variance. GroEL (*MAB_0650*) and Acyl-CoA dehydrogenase FadE (*MAB_4437*) had the greatest PC1 and PC2 coefficients, respectively. **c** Percentage of proteins with misincorporation of L-norvaline at leucine residues from cell lysates after 24 h of growth in Sauton's media with 0.5 mM L-norvaline. Data are median with IQR, whiskers represent 1–99 percentile from spectral counting. *P* values were obtained by Friedman test with Dunn's multiple comparisons test. **d** Volcano plots depict fold change (log_2) and *P* value($-log_{10}$) for each protein relative to the ATCC 19977 reference strain.

while the editing-deficient strain *M. abscessus* EPT^R D436H had a significant increase in norvaline misincorporation (Fig. 4c and Supplementary Fig. 5a). *M. abscessus* EPT^R Nva^R 4XSS reduced the median level of norvaline misincorporation significantly despite lacking LeuRS editing activity (Fig. 4c and Supplementary Fig. 5a). A decrease in median norvalination was also observed in the strain complemented with mutant *leuA* but not with the wild-type *leuA* control (Fig. 4c). We also measured the level of L-norvaline in the culture supernatants after 24 h of exposure and found no evidence of L-norvaline degradation or modification (Supplementary Fig. 5b). To assess the overall bacterial stress response to L-norvaline challenge, we compared the proteomes of *M. abscessus* EPT^R D436H, complemented strains, and *M. abscessus* EPT^R Nva^R 4×SS to the ATCC 19977 reference strain. Higher levels of norvaline incorporation resulted in 134 statistically significant differentially expressed proteins (DEPs) (Fig. 4d). While *M. abscessus* EPT^R D436H had elevated levels of heat shock proteins and Clp proteases relative to the ATCC 19977 strain, we observed a significantly attenuated stress response in *M. abscessus* EPT^R Nva^R 4×SS with 10 DEPs and in *M. abscessus* EPT^R D436H complemented with α-IPMS^{A555V} with 28 DEPs (Fig. 4d).

α-IPMS^{A555V} mutation located in allosteric site

To understand how the α-IPMS^{A555V} substitution resulted in minimal L-norvaline misincorporation across the proteome, we modelled α-IPMS$_{Mabs}$ onto the experimentally determined structure of α-IPMS$_{Mtb}$ using Swiss-Model[48]. The current understanding is that the catalytic and regulatory domains are separated by a flexible hinge domain to accommodate conformational changes resulting from L-leucine bound in the allosteric site to elicit negative feedback inhibition[48]. As a control, we compared the experimental structure of α-IPMS$_{Mtb}$ (PDB 3FIG) to the α-IPMS$_{Mtb}$ structure generated with Swiss-Model. We generated a homodimeric structure (QMEAN 0.87 ± 0.05) that was predicted to have the N-terminal catalytic $(\alpha/\beta)_8$ TIM barrel domain, a linker, and C-terminal regulatory domain with the ββββα architecture (Supplementary Fig. 6a). Next, we compared the overlaid structures of Swiss-Model generated α-IPMS$_{Mtb}$ and α-IPMS$_{Mabs}$ and observed substantial structural overlap with rmsd of 0.119 Å. From these results, we inferred homology between α-IPMS$_{Mtb}$ and α-IPMS$_{Mabs}$ and used the experimental α-IPMS$_{Mtb}$ structure to hypothesize the effect of α-IPMS^{A555V} substitution identified in *M. abscessus* EPT^R Nva^R 4×SS.

The experimentally determined structure of α-IPMS$_{Mtb}$ was solved as a homodimer with an N-terminal catalytic domain and a C-terminal regulatory domain (Fig. 5a, PDB 3FIG and 3HPZ). The regulatory domains contain two symmetrical pockets at the dimer interface with loops in an open conformation when unbound to L-leucine (Fig. 5b, PDB 3HPZ)[48]. However, the loop adopts a closed conformation when L-leucine is bound in the hydrophobic pocket of the regulatory domain (Fig. 5c, PDB 3FIG)[48]. The A555V substitution identified from WGS in *M. abscessus* EPT^R Nva^R 4XSS is located on this loop (Fig. 5c). We modelled the A555V substitution on α-IPMS$_{Mabs}$ and observed a deviation >4σ from the ideal angle with D557 and S554 was identified as a rotamer outlier. Taken together with the additional electron density from A555V next to the side chain of L546, we hypothesized that A555V would prevent the loop from adopting a closed conformation when bound by L-leucine and disrupt the allosteric feedback inhibition.

Overproduction of L-leucine competitively inhibits L-norvaline

To understand the mechanism of L-norvaline resistance in the absence of LeuRS editing activity, we hypothesized that the mutation in α-IPMS would disrupt the equilibrium of the L-leucine biosynthetic pathway and confer abnormal L-leucine production through loss of allosteric regulation in α-IPMS (Fig. 5d). To test this hypothesis, we grew *M. abscessus* ATCC 19977, *M. abscessus* EPT^R D436H, complemented strains, and *M. abscessus* EPT^R Nva^R 4XSS in Sauton's minimal media and measured the concentration of BCAAs in the culture filtrate using HPLC/MS. Indeed, *M. abscessus* strains that harboured α-IPMS^{A555V} produced higher concentrations of L-leucine relative to the ATCC 19977 reference strain while L-isoleucine concentrations were unaffected (Fig. 5e). L-Valine concentrations, however, were significantly reduced in strains that produced excess L-leucine (Fig. 5e and Supplementary Fig. 7).

Next, we examined the rescue effect of L-leucine by growing *M. abscessus* EPT^R D436H in 0.5 mM L-norvaline with increasing L-leucine concentrations. After day 7 of growth, we observed that a 1:1 ratio of L-leucine:L-norvaline restored the growth of *M. abscessus* EPT^R D436H to 50% of the L-norvaline free conditions while L-isoleucine and L-valine had no rescue effect (Fig. 5f). Growth was completely restored with a 4:1 ratio of L-leucine:L-norvaline (Fig. 5f). Motivated by these results, we asked whether L-leucine could act as a competitive inhibitor to L-norvaline. We measured the initial growth rates from time 0 to 24 h in serial dilutions of L-norvaline to generate a dose-response curve (Fig. 5g). These measurements were repeated with increasing L-leucine concentrations and required higher concentrations of norvaline to generate saturating growth inhibition. To obtain IC_{50} values for L-norvaline, the saturating curves were fit to four parameter dose–response regression. Next, IC_{50} values were used to estimate an apparent inhibition constant of L-norvaline, K_i, and an apparent substrate constant of L-leucine, K_s, using the Cheng–Prusoff theorem for competitive inhibition (Fig. 5h). The linear relationship between the IC_{50} of L-norvaline and the concentration of L-leucine suggests competitive inhibition between the amino acids where L-norvaline (K_i = 9 μM) is 3-4x more potent as an inhibitor than L-leucine (K_s = 32 μM) is as a substrate (Fig. 5h).

DISCUSSION

M. abscessus infections are notoriously difficult to treat largely due to its enhanced toolkit of antimicrobial resistance mechanisms[6]. We show that *M. abscessus* can subvert the toxicity of L-norvaline, a non-canonical amino acid shown to be an experimental adjunct agent with epetraborole[29]. Classically, *M. abscessus* is naturally resistant to L-norvaline because of the editing domain on LeuRS. LeuRS provides pre-transfer editing before the incorrect amino acid is transferred to tRNA^{Leu} or post-transfer editing when the erroneous amino acid has already been transferred onto tRNA^{Leu} [49]. In both mechanisms, the editing activity is mediated by a conserved aspartic acid residue, D436. Our results demonstrate that a *M. abscessus* mutant can limit the incorrect use of L-norvaline in the absence of pre- and post-transfer editing activity. We show that resistance is not the result of modified membrane hydrophobicity nor increased efflux activity but stems from the loss of allosteric regulation to overproduce a metabolite and outcompete the inhibitor.

The A555V mutation was found in α-IPMS, the first enzyme involved in L-leucine biosynthesis[50]. α-IPMS was previously shown to have a regulatory domain with a hydrophobic pocket where L-leucine binds with the carboxylate positioned between the partial positively charged N-terminal ends of two helices, similar to the bound chloride ion in the absence of L-leucine[48]. From the crystal structure, it was hypothesized to be a regulatory domain for feedback inhibition. Later, kinetic evidence emerged that supported intradomain communication by an allosteric mechanism with L-leucine[51]. This regulation had also been postulated in yeast where mutations were identified in the C-terminal regulatory domain that resulted in insensitivity to L-leucine feedback inhibition[52]. Other non-regulatory yeast α-IPMS mutants became resistant to Zn^{2+}-mediated inactivation by coenzyme-A. This was later supported with kinetic data examining the effects of divalent cations on the activity of α-IPMS as a mechanism to control energy metabolism[52,53].

In line with the allosteric mechanism of α-IPMS, our results show an increased production of L-leucine by strains harbouring α-IPMS^{A555V} relative to the ATCC 19977 reference strain. We also tested L-isoleucine and observed no difference in BCAA production. L-Valine, however, was significantly reduced in strains that produced more L-leucine. Although BCAAs share structural features, the biosynthetic pathway for L-isoleucine is dependent on L-threonine production while L-leucine/L-valine are synthesized from pyruvate. The α-IPMS negative feedback mechanism is believed to be specific for L-leucine since α-IPMS catalyses the first committed step of L-leucine biosynthesis after diverging away from the shared L-valine pathway[50]. L-Isoleucine and L-valine have also been shown to be allosteric inhibitors and activators, respectively, but towards the L-isoleucine chokepoint enzyme, threonine deaminase[54]. Unregulated α-IPMS activity that shifts the equilibrium of 2-oxoisovalerate could explain why L-valine production was stunted in strains with α-IPMS^{A555V}.

M. abscessus grown under L-norvaline challenge showed that α-IPMS^{A555V} strains were more resistant to growth inhibition than α-IPMS^{WT} strains. Strains with LeuRS^{D436H} fail to grow in 0.5 mM L-norvaline however, the natural double mutant *M. abscessus* EPT^R

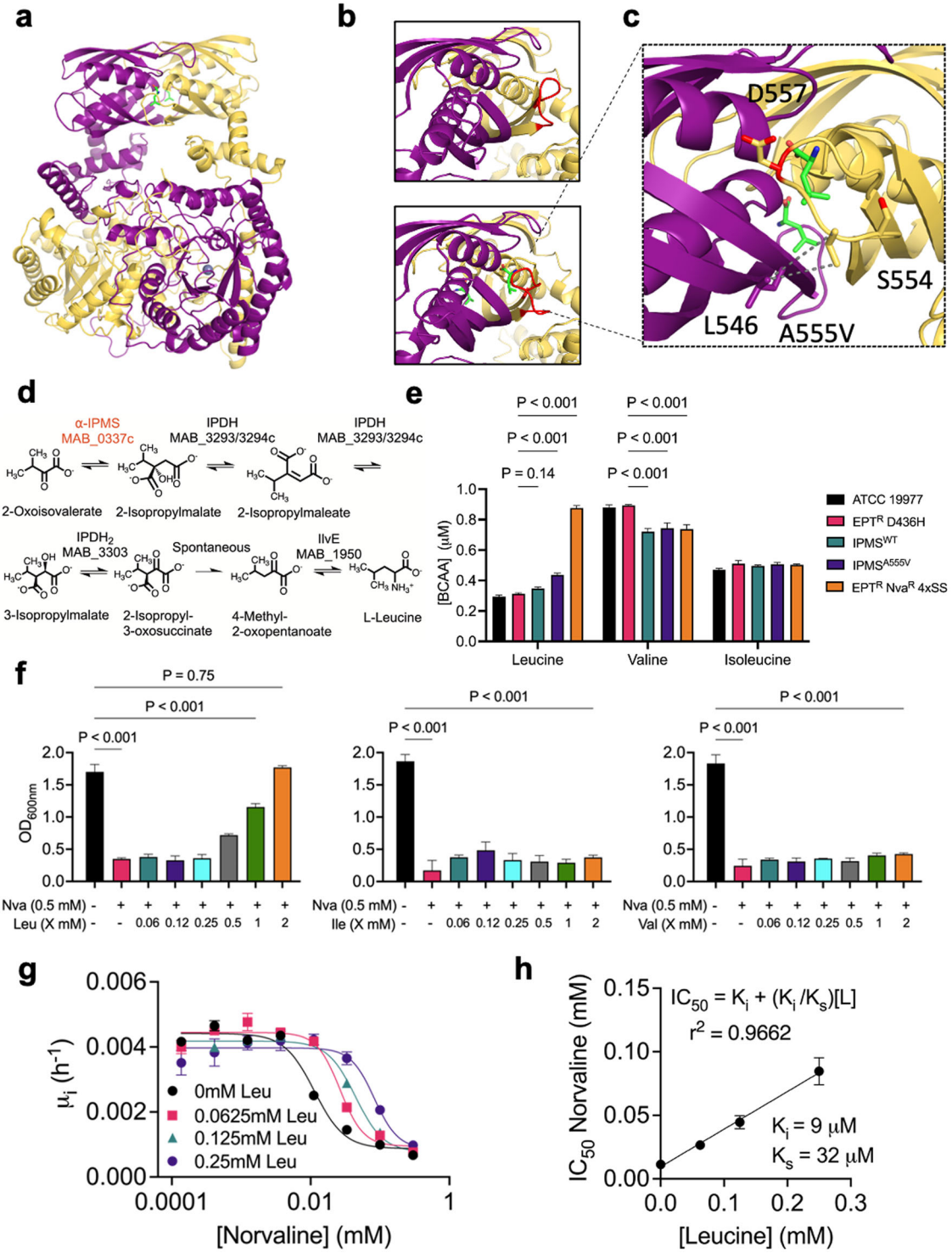

Fig. 5 α-IPMS^{A555V} variant over produces L-leucine to outcompete L-norvaline. **a** Swiss-Model structure of α-IPMS$_{Mabs}$ from *M. tuberculosis* PDB 3FIG[48]. Monomers in yellow and purple, L-leucine in green, and Zn^{2+} as blue spheres. **b** (upper) C-terminal regulatory domain without L-leucine bound in an open conformation (red loop). **b** (lower) C-terminal regulatory domain with L-leucine bound in a closed conformation. **c** Effects of mutated A555V highlighted. **d** Pathway for L-leucine synthesis. **e** BCAA concentrations in culture filtrates of reference strain ATCC 19977, EPT^R D436H, EPT^R D436H complemented with IPMS^{WT} or IPMS^{A555V}, and naturally raised EPT^R Nva^R 4×SS mutant grown in Sauton's minimal media. Data are mean ± SD of $n = 3$ biological replicates. *P* values were obtained by one-way ANOVA with Tukey's multiple comparisons test. **f** *M. abscessus* EPT^R D436H strain grown in Sauton's minimal media ± L-norvaline and serial dilutions of L-leucine, L-isoleucine, or L-valine. Data are mean ± SD of $n = 3$ independent experiments. *P* values were obtained by one-way ANOVA with Tukey's multiple comparisons test. **g** Initial growth rates (first 24 h) of *M. abscessus* EPT^R D436H in L-norvaline supplemented with L-leucine. **h** L-norvaline inhibition fit to a model of competitive inhibition. K_i is the inhibition constant of L-norvaline. K_s is the substrate constant for L-leucine. *L* is the concentration of L-leucine.

Nva^R 4×SS and *M. abscessus* EPT^R D436H complemented with α-IPMS^{A555V} had comparable growth to *M. abscessus* ATCC 19977. These data suggest that overproduction of L-leucine from the mutation in the loop capping the allosteric site results in resistance to L-norvaline. The growth kinetics of *M. abscessus* EPT^R D436H in L-norvaline and L-leucine shed light on the requirement for additional L-leucine and the biochemical basis for L-leucine rescue. By measuring initial growth rates, we observed increasing L-norvaline IC_{50} values proportional to the L-leucine concentration, suggestive of competitive inhibition with $K_i = 9$ μM for L-norvaline and $K_s = 32$ μM for L-leucine. The inhibition and substrate constants lend additional support to the L-leucine rescue experiments where nearly 4× more L-leucine was required to fully restore the growth of *M. abscessus* EPT^R D436H in 0.5 mM L-norvaline.

Corroborating our previous results, strains that produced higher levels of L-leucine and misincorporated less L-norvaline in the proteome had superior growth output in L-norvaline. The proteomic profiles suggest that strains with α-IPMS^{A555V} can tolerate L-norvaline as the unfolded protein response observed in *M. abscessus* EPT^R D436H, characterized by heat shock proteins and chaperonins in the dominant principal component 1, is diminished in *M. abscessus* EPT^R Nva^R 4×SS. The variance in principal component 2 is attributed to an increased FadE abundance in strains that failed to grow during norvaline challenge. FadE is predicted to be an acyl-CoA dehydrogenase involved in fatty acid β-oxidation, which suggests that *M. abscessus* EPT^R D436H and α-IPMS^{wt} complemented strain upregulated fatty acid β-oxidation to meet the metabolic requirements of misfolded protein proteolysis. Overall, the proteome of strains with α-IPMS^{A555V} clustered separately from *M. abscessus* EPT^R D436H and appeared more similar to the ATCC 19977 reference strain.

In conclusion, we describe an unconventional mechanism of resistance to an antimicrobial agent. Systematic evaluation revealed that the *M. abscessus* resistance phenotype was due to the loss of allosteric feedback inhibition in a biosynthetic enzyme. *M. abscessus* expressing α-IPMS^{A555V} gained the ability to produce excess quantities of L-leucine, with no deleterious consequences, to outcompete L-norvaline from being used as a LeuRS substrate. This mutation reduces norvalination of the proteome and toxicity associated with misfolded proteins. Our work here provides evidence for a mechanism of antimicrobial resistance in *M. abscessus* where an orthogonal mutation in an allosteric choke-point enzyme rescues the bacteria through dysregulation of BCAA metabolism.

METHODS

Culture conditions

M. abscessus strains were grown in rolling liquid culture at 37 °C in Middlebrook 7H9 (Difco) supplemented with 10% (v/v) albumin dextrose catalase (ADC), 0.2% (v/v) glycerol, and 0.05% (v/v) Tween 80 (7H9 complete) or Sauton's defined minimal media. 7H10 agar plates supplemented with 10% (v/v) oleic acid ADC (OADC) and 0.5% (v/v) glycerol were used for growth on solid media at 37 °C.

Norvaline time-dependent killing

Log phase (OD_{600} of 0.4–0.8) *M. abscessus* was diluted to an OD_{600} of 0.0001 (10^5 CFU/mL) and challenged with an initial dose of L-norvaline at 4× MIC_{90} of the sensitive *M. abscessus* LeuRS^{D436H} strain or norvaline at 4× MIC_{90} supplemented daily to create steady-state conditions (4×SS). One hundred microlitres aliquots were taken and serially diluted in 7H9 complete and plated on 7H10 agar. The starting inoculum was determined from time 0 before norvaline was added. CFUs were determined after 4 days of incubation at 37 °C. Bactericidal activity is defined as a 3 $\log_{10}$ decrease (99.9%) from the starting inoculum.

Minimum inhibitory concentrations (MIC)

MIC values were determined using the resazurin microtiter assay (REMA). Cultures were grown to log phase (OD_{600} of 0.4–0.8) and diluted to OD_{600} of 0.005 (5×10^5 CFU/mL). Compounds were prepared in twofold serial dilutions in 96-well plates with 90 μL of bacteria per well to a final volume of 100 μL. 96-well clear, flat bottom plates were incubated at 37 °C until drug-free wells were turbid (2 days for *M. abscessus*). Ten microliters of resazurin prepared at 0.025% (w/v) in distilled water was added to each well. Once the drug-free wells turned pink (3–4 h or one doubling time), the fluorescence (Ex/Em 560/590) was measured using an Infinite F200 Tecan plate reader. Fluorescence intensities were converted to percentage of viable cells relative to drug-free conditions and fit to the modified four-parameter dose-response regression using GraphPad Prism version 9. MIC values at 90% reduction of viability were determined from the Gompertz nonlinear regression equation[55].

Isolating L-norvaline-resistant mutants

L-norvaline-resistant mutants of *M. abscessus* ATCC 19977 were isolated from L-norvaline time-dependent killing assays. Single colonies were obtained from streaked 7H10 plates. Genomic DNA (gDNA) was extracted from *M. abscessus* EPT^R LeuRS^{D436H} as the parental strain and two colonies of *M. abscessus* EPT^R Nva^R 4×SS mutants with confirmed norvaline resistance (REMA method) using the Qiagen QiaAMP UCP Pathogen mini kit with a modified mechanical lysis protocol. Culture was pelleted by centrifugation and resuspend in 590 μL of ATL buffer containing the Dx reagent in a low-bind tube. Forty microlitres of proteinase K (20 mg/mL) and 20 μL of lysozyme (100 mg/mL) were added and incubated for 30 min at 56 °C under agitation. Solution was transferred into a Pathogen Lysis Tube L and vortexed twice using a FastPrep-24 instrument at 6.5 m/s for 45 s with a 5-min incubation on ice in between. Supernatant was transferred into a fresh 2 mL low-bind tube and gDNA was collected via spin protocol according to manufacturer's instructions. gDNA was quantified with Quant-iT PicoGreen dsDNA kit.

Sequencing and variant calling

Paired-end read sequencing libraries were prepared using Illumina S4 kit. Whole genome sequencing was performed on Illumina Novaseq 6000. Raw paired-end reads were adaptor and quality trimmed with Trimmomatic v0.40 and aligned to the *M. abscessus* ATCC 19977 reference genome (GenBank: CU_458896.1) using Burrows-Wheeler Aligner - maximum exact matches algorithm (bwa-mem)[56,57]. Aligned reads were sorted using SAMTOOLs[58]. Duplicate reads were filtered using Picard. Freebayes v1.3.6 was used for variant calling and filtering variants with mapping quality 60, minimum coverage 10, minimum allele frequency of 0.5, and QUAL > 100 [59]. Variants identified in parental and resistant strains were manually compared to isolate variants unique to resistant strains.

Growth curves

Bacteria were grown to log phase (OD_{600} of 0.4–0.8) in 7H9 complete or Sauton media and diluted to OD_{600} of 0.005 (5×10^6 CFU/mL). Branched-chain amino acids (BCAAs) were added to 90 μL of bacteria to a final volume of 100 μL. Growth curves were performed in 96-well clear, flat bottom microtiter plates, incubated statically at 37 °C before measuring A_{600} on an Infinite F200 Tecan plate reader. Data was fit to an exponential plateau regression to determine the growth rate μ and maximum growth plateau Y_M. Alternatively, strains were grown on 7H10 agar plates

with different BCAAs. For each strain in a particular BCAA, CFUs were enumerated and reported as a percentage relative to the CFUs enumerated in the regular 7H10 agar plates.

Congo red uptake

Strains were grown on 7H10 agar plates supplemented with 10% (v/v) OADC, 0.5% (v/v) glycerol, and Congo red at 140 µM at 37 °C. After 5 days, cells were scraped into an Eppendorf tube and washed with water until the supernatant turned clear. Washed cells were incubated with 1 mL of DMSO for 2 h. Supernatants were collected and measured at A_{488} using an Infinite F200 Tecan plate reader. Values were normalized to the dry weight of the pellet.

Ethidium bromide efflux

M. abscessus strains were grown to log phase (OD_{600} of 0.4–0.8) in Sauton media and diluted to OD_{600} of 0.2. Eighty microliters of bacteria was added to a black, clear bottom 96-well plate with 10 µL serially diluted ethidium bromide and 10 µL of media. For efflux pump inhibition assays, media was replaced with 10 µL of verapamil or carbonyl cyanide m-chlorophenyl hydrazone (CCCP) for a final concentration of 0.5 mM or 25 µM, respectively. Fluorescence (Ex/Em 525/600) was measured every 90 s for 2 h at 25 °C using an Infinite F200 Tecan plate reader.

Cloning and over-expressing *leuA* in *M. abscessus* EPT^R $LeuRS^{D436H}$

The wildtype and mutant *leuA* gene (*MAB_0337c*), which encodes α-isopropylmalate synthase, and $tRNA^{Leu(GAG)}$ gene (*MAB_t5031c*), which encodes one of five tRNA isoacceptors in *M. abscessus*, were PCR amplified from gDNA including 250 bp upstream to capture the native promoters using Q5 polymerase with forward $primer_{leuA}$ (5′ ACTGCAGAATTCTCCTTGAGAGCGCTCGCGAAG) and reverse $primer_{leuA}$ (5′ GATGATAAGCTTCTAGGCGCGAGCAG-CACGG), and forward $primer_{tRNA}$ (5′ ACTGCAGAATTCGGTGTTG-GAGGTGTCGAAACGG) and reverse $primer_{tRNA}$ (5′ GATGATAAGCTTTGTCCGAGGGGGGACTTGAAC). PCR products and the *E. coli*/mycobacterial shuttle vector pMV306_hsp60 were digested with EcoRV and HindIII restriction enzymes, ligated, and transformed into *E. coli* DH5*α* cells (Promega). Plasmids were extracted and sequenced using Sanger sequencing. Sequence confirmed constructs were electroporated into the parental strain *M. abscessus* EPT^R D436H. An empty pMV306_hsp60 vector was included as a control. *M. abscessus* EPT^R D436H complemented with wild type *leuS* was described previously[29].

Initial growth kinetics and data theory

M. abscessus strains were grown to log phase (OD_{600} of 0.4-0.8) in Sauton media and diluted to OD_{600} of 0.005 in 96-well clear, flat bottom microtiter plates with serial dilutions of norvaline. Each set of norvaline dose–response curves was incubated with a constant amount of L-leucine as a norvaline inhibitor. Plates were incubated statically at 37 °C and A_{600} was measured on an Infinite F200 Tecan plate reader to monitor growth. Initial growth rates, μ_i (h^{-1}), were measured during the first 24 h of growth. Growth rate inhibition, performed under variable norvaline concentrations and constant L-leucine concentrations (0 mM, 0.0625 mM, 0.125 mM, or 0.250 mM), were fitted to a dose–response curve

$$\mu = \mu_{min} - (\mu_{max} - \mu_{min})/[1 + (I/IC_{50})^{n_H}], \quad (1)$$

where μ is the rate in the presence of inhibitor at concentration I, μ_{max}, and μ_{min} are the maximum and minimum growth rates, IC_{50} is the concentration of inhibitor that inhibits the growth rate by 50%, and n_H is the Hill coefficient. IC_{50} values were used to estimate an apparent inhibition constant, K_i, using the Cheng-Prusoff equation for competitive inhibition

$$K_i = IC_{50}/(1 + L/K_s), \quad (2)$$

where K_i is the apparent inhibition constant for norvaline, L is the concentration of L-leucine, and K_s is the substrate affinity constant of L-leucine.

LC-MS/MS measurement of norvaline in the proteome

M. abscessus strains were grown to early log phase (OD_{600} of 0.1–0.2) and challenged with 0.5 mM L-norvaline in Sauton media for 24 h. Proteins were extracted using an optimized protocol for mass spectrometry follow-up[60]. Cells were collected, washed with ice-cold PBS, and resuspended in 1 mL lysis buffer (50 mM NH_4HCO_3 pH 7.4, 10 mM $MgCl_2$, 0.1% NaN_3, 1 mM EGTA, 1× protease inhibitors (Roche), 7 M urea, and 2 M thiourea). Cells were lysed with zirconia beads and the cell lysate was collected and filtered through a 0.22 µm membrane. Proteins were precipitated overnight at 4 °C with TCA at 25% (v/v). The precipitate was washed with 1 mL cold acetone and 250 µL cold water. The final wash is only water. The pellet was resuspended in 200 µL resuspension buffer (50 mM NH_4HCO_3, 1 M urea). Protein extraction was quantified with the Bradford assay and the quality of proteins was examined on SDS-PAGE. Protein lysates were dissolved in SDS-PAGE reducing buffer and electrophoresed onto a single stacking gel band to remove lipids, detergents and salts. For each sample, a single gel band was reduced with DTT (Sigma), alkylated with iodoacetic acid (Sigma) and digested with LC-MS grade trypsin (Promega). Extracted peptides were re-solubilized in 0.1% aqueous formic acid and loaded onto a Thermo Acclaim Pepmap (Thermo, 75 µM ID × 2 cm C18 3 µM beads) precolumn and then onto an Acclaim Pepmap Easyspray (Thermo, 75 µM × 15 cm with 2 µM C18 beads) analytical column separation using a Dionex Ultimate 3000 uHPLC at 250 nl/min with a gradient of 2–35% organic (0.1% formic acid in acetonitrile) over 2 h. Peptides were analysed using a Thermo Orbitrap Fusion mass spectrometer operating at 120,000 resolution for MS1 with HCD sequencing at top speed (15,000 resolution) for all peptides with a charge of 2+ or greater. The raw data were converted into *.mgf format (Mascot generic format) for searching using the Mascot 2.5.1 search engine (Matrix Science) against *M. abscessus* protein sequences (Uniprot downloaded 2020.11.30). A modification for Xle->Val was used to detect incorporation of Val into wild-type sequences. The database search results were loaded onto Scaffold Q + Scaffold_4.4.8 (Proteome Sciences) for statistical treatment and data visualization.

Principal component analysis

The dataset comprised of the 1000 most abundant proteins from each strain of *M. abscessus* based on quantitative spectral counts. Spectral counts for each protein were standardized within strains. Principal component analysis (PCA) was performed using R to generate the loading data and scores. PCA was visualized with the first two principal components which accounted for >95% of the variance.

LC-MS measurement of BCAA

Samples aliquots were diluted with an internal standard (norvaline-d5) and derivatized with 6-aminoquinolyl-*N*-hydroxysuccinimidyl carbamate (AQC; Toronto Research Chemicals, ON, Canada) for analysis using reversed phase ultra performance liquid chromatography mass spectrometry (UPLC-MS). Samples were prepared and analysed along with calibration curves containing isoleucine, leucine, norvaline and valine (Sigma-Aldrich, St. Louis, MO, USA) in culture media. An internal standard working solution (ISWS) containing 50 µM norvaline-d5 (CDN Isotopes, Dorval, QC, Canada) in water was added to the experimental and calibration

samples prior to derivatization. ISWS aliquots (25 µL) were added to sample aliquots (25 µL) in microcentrifuge tubes and vortexed. Aliquots (10 µL) then were transferred into glass tubes containing 70 µL buffer solution (0.2 M sodium borate pH 8.8) along with 20 µL derivatization solution (10 mM AQC in acetonitrile), mixed and incubated for 10 min at 55 °C. After cooling to room temperature, aliquots (5 µL) were transferred to autosampler vials containing 995 µL Type-1 water for UPLC-MS analysis. Samples were analysed by UPLC-MS using an Agilent 6460 triple quadrupole mass spectrometer coupled with an Agilent 1290 UPLC system (Agilent, Santa Clara, California, USA). Samples (5 µL) were injected onto an Agilent Eclipse Plus C18 100 × 2.1 mm (1.8 µm) column and chromatographed with a reverse phase gradient at 0.250 mL/min using 0.1% formic acid in water and 0.1% formic acid in acetonitrile. The derivatized amino acids were detected using electrospray positive mode ionization followed by MS/MS fragmentation. Data acquisition was performed using the Agilent MassHunter Data Acquisition (version B.04.01) software. Peak area measurements from selected product ions, calibration curve regression analysis and resulting sample quantification were performed using the Agilent MassHunter Quantitative Analysis (version B.05.00) software.

Homology modelling

The models of α-IPMS$_{Mabs}$ (*MAB_0337c*) were generated using the SWISS-MODEL server and the crystal structures of α-IPMS$_{Mtb}$ as templates (PDB 3FIG, 3HPZ)[61,62].

Data analysis

Data were processed by GraphPad PRISM 9.4.1, The PyMOL Molecular Graphics System 2.3.0, R 4.1.2, and Scaffold Q + Scaffold_4.4.8.

Reporting summary

Further information on research design is available in the Nature Research Reporting Summary linked to this article.

DATA AVAILABILITY

The datasets used and/or analysed during the current study are available from the corresponding author on reasonable request. Sequence data has been deposited in the NCBI Sequence Read Archive under the NCBI BioProject ID PRJNA950212.

Received: 14 December 2022; Accepted: 18 April 2023;
Published online: 03 July 2023

REFERENCES

1. World Health Organisation. *WHO Strategic Priorities on Antimicrobial Resistance* (WHO, 2022).
2. Murray, C. J. et al. Global burden of bacterial antimicrobial resistance in 2019: a systematic analysis. *Lancet* **399**, 629–655 (2022).
3. Cassini, A. et al. Attributable deaths and disability-adjusted life-years caused by infections with antibiotic-resistant bacteria in the EU and the European Economic Area in 2015: a population-level modelling analysis. *Lancet Infect. Dis.* **19**, 56–66 (2019).
4. World Health Organization. *Prioritization of Pathogens to Guide Discovery, Research and Development of New Antibiotics for Drug-Resistant Bacterial Infections, Including Tuberculosis*. *WHO/EMP/IAU/2017.12* (WHO, 2017).
5. Burki, T. K. Tuberculosis missing from WHO bacteria list. *Lancet Respir. Med.* **5**, 252 (2017).
6. Nessar, R., Cambau, E., Reyrat, J. M., Murray, A. & Gicquel, B. *Mycobacterium abscessus*: a new antibiotic nightmare. *J. Antimicrob. Chemother.* **67**, 810–818 (2012).
7. Pasipanodya, J. G. et al. Systematic review and meta-analyses of the effect of chemotherapy on pulmonary *Mycobacterium abscessus* outcomes and disease recurrence. *Antimicrob. Agents Chemother.* **61**, e01206-17 (2017).
8. Dartois, V. & Dick, T. Drug development challenges in nontuberculous mycobacterial lung disease: TB to the rescue. *J. Exp. Med.* **219**, e20220445 (2022).
9. Quang, N. T. & Jang, J. Current molecular therapeutic agents and drug candidates for *Mycobacterium abscessus*. *Front. Pharmacol.* **12**, 724725 (2021).
10. Dartois, V. A. & Rubin, E. J. Anti-tuberculosis treatment strategies and drug development: challenges and priorities. *Nat. Rev. Microbiol.* **60**, 685–701 (2022).
11. Wallace, R. J. et al. Genetic basis for clarithromycin resistance among isolates of *Mycobacterium chelonae* and *Mycobacterium abscessus*. *Antimicrob. Agents Chemother.* **40**, 1676–1681 (1996).
12. Jarlier, V. & Nikaido, H. Permeability barrier to hydrophilic solutes in *Mycobacterium chelonei*. *J. Bacteriol.* **172**, 1418–1423 (1990).
13. Jarlier, V. & Nikaido, H. Mycobacterial cell wall: structure and role in natural resistance to antibiotics. *FEMS Microbiol. Lett.* **123**, 11–18 (1994).
14. Adams, R. A. et al. Rifamycin antibiotics and the mechanisms of their failure. *J. Antibiot.* **74**, 786–798 (2021).
15. Schäfle, D. et al. Rifabutin is inactivated by *Mycobacterium abscessus* Arr. *Antimicrob. Agents Chemother.* **65**, e02215-20 (2021).
16. Ung, K. L., Alsarraf, H. M. A. B., Olieric, V., Kremer, L. & Blaise, M. Crystal structure of the aminoglycosides N-acetyltransferase Eis2 from *Mycobacterium abscessus*. *FEBS J* **286**, 4342–4355 (2019).
17. Luthra, S., Rominski, A. & Sander, P. The role of antibiotic-target-modifying and antibiotic-modifying enzymes in *Mycobacterium abscessus* drug resistance. *Front. Microbiol.* **9**, 2179 (2018).
18. Hamad, B. The antibiotics market. *Nat. Rev. Drug Discov.* **9**, 675–676 (2010).
19. Story-Roller, E., Maggioncalda, E. C., Cohen, K. A. & Lamichhane, G. *Mycobacterium abscessus* and β-Lactams: emerging insights and potential opportunities. *Front. Microbiol.* **9**, 2273 (2018).
20. Ramírez, A. et al. Biochemical characterization of β-lactamases from *Mycobacterium abscessus* complex and genetic environment of the β-lactamase-encoding gene. *Microb. Drug Resist.* **23**, 294–300 (2017).
21. Burian, J. et al. The mycobacterial transcriptional regulator whiB7 gene links redox homeostasis and intrinsic antibiotic resistance. *J. Biol. Chem.* **287**, 299–310 (2012).
22. Burian, J. et al. The mycobacterial antibiotic resistance determinant WhiB7 acts as a transcriptional activator by binding the primary sigma factor SigA (RpoV). *Nucleic Acids Res.* **41**, 10062–10076 (2013).
23. Hurst-Hess, K., Rudra, P. & Ghosh, P. *Mycobacterium abscessus* WhiB7 regulates a species-specific repertoire of genes to confer extreme antibiotic resistance. *Antimicrob. Agents Chemother.* **61**, e01347-17 (2017).
24. Richard, M., Gutiérrez, A. V. & Kremer, L. Dissecting erm(41)-mediated macrolide-inducible resistance in *Mycobacterium abscessus*. *Antimicrob. Agents Chemother.* **64**, e01879-19 (2020).
25. Pryjma, M., Burian, J., Kuchinski, K. & Thompson, C. J. Antagonism between front-line antibiotics clarithromycin and amikacin in the treatment of *Mycobacterium abscessus* infections is mediated by the whiB7 gene. *Antimicrob. Agents Chemother.* **61**, e01353-17 (2017).
26. Nash, K. A., Brown-Elliott, A. B. & Wallace, R. J. A Novel gene, erm(41), confers inducible macrolide resistance to clinical isolates of *Mycobacterium abscessus* but is absent from *Mycobacterium chelonae*. *Antimicrob. Agents Chemother.* **53**, 1367–1376 (2009).
27. Brennan, P. J. Structure, function, and biogenesis of the cell wall of *Mycobacterium tuberculosis*. *Tuberculosis* **83**, 91–97 (2003).
28. Brennan, P. J. & Nikaido, H. The envelope of mycobacteria. *Annu. Rev. Biochem.* **64**, 29–63 (1995).
29. Sullivan, J. R. et al. Efficacy of epetraborole against *Mycobacterium abscessus* is increased with norvaline. *PLoS Pathog* **17**, 1–28 (2021).
30. O'Dwyer, K. et al. Bacterial resistance to leucyl-tRNA synthetase inhibitor GSK2251052 develops during treatment of complicated urinary tract infections. *Antimicrob. Agents Chemother.* **59**, 289–298 (2015).
31. Nandi, P. & Sen, G. An antifungal substance from a strain of *B. subtilis*. *Nature* **172**, 871–872 (1953).
32. Kisumi, M., Sugiura, M. & Chibata, I. Biosynthesis of norvaline, norleucine, and homoisoleucine in *Serratia marcescens*. *J. Biochem.* **80**, 333–339 (1976).
33. Apostol, I. et al. Incorporation of norvaline at leucine positions in recombinant human hemoglobin expressed in *Escherichia coli*. *J. Biol. Chem.* **272**, 28980–28988 (1997).
34. Soini, J. et al. Norvaline is accumulated after a down-shift of oxygen in *Escherichia coli* W3110. *Microb. Cell Fact.* **7**, 30 (2008).
35. Alvarez-Carreño, C., Becerra, A. & Lazcano, A. Norvaline and norleucine may have been more abundant protein components during early stages of cell evolution. *Orig. Life Evol. Biosph.* **43**, 363–375 (2013).
36. Cvetesic, N., Palencia, A., Halasz, I., Cusack, S. & Gruic-Sovulj, I. The physiological target for Leu RS translational quality control is norvaline. *EMBO J.* **33**, 1639–1653 (2014).

37. Ganapathy, U. S., Gengenbacher, M. & Dick, T. Epetraborole is active against *Mycobacterium abscessus*. *Antimicrob. Agents Chemother.* **65**, e0115621 (2021).
38. Svetlov, M. S. et al. Structure of Erm-modified 70S ribosome reveals the mechanism of macrolide resistance. *Nat. Chem. Biol.* **17**, 412–420 (2021).
39. Viljoen, A., Viela, F., Kremer, L. & Dufrêne, Y. F. Fast chemical force microscopy demonstrates that glycopeptidolipids define nanodomains of varying hydrophobicity on mycobacteria. *Nanoscale Horizons* **5**, 944–953 (2020).
40. Viljoen, A. et al. The diverse family of MmpL transporters in mycobacteria: from regulation to antimicrobial developments. *Mol. Microbiol.* **104**, 889–904 (2017).
41. Xu, Z., Meshcheryakov, V. A., Poce, G. & Chng, S. S. MmpL3 is the flippase for mycolic acids in mycobacteria. *Proc. Natl Acad. Sci. USA* **114**, 7993–7998 (2017).
42. Hartkoorn, R. C., Uplekar, S. & Cole, S. T. Cross-resistance between clofazimine and bedaquiline through upregulation of mmpl5 in *Mycobacterium tuberculosis*. *Antimicrob. Agents Chemother.* **58**, 2979–2981 (2014).
43. Gutiérrez, A. V., Richard, M., Roquet-Banères, F., Viljoen, A. & Kremer, L. The TetR family transcription factor MAB_2299c regulates the expression of two distinct MmpS-MmpL efflux pumps involved in cross-resistance to clofazimine and bedaquiline in *Mycobacterium abscessus*. *Antimicrob. Agents Chemother.* **63**, e01000-19 (2019).
44. Machado, D. et al. Efflux activity differentially modulates the levels of isoniazid and rifampicin resistance among multidrug resistant and monoresistant *Mycobacterium tuberculosis* strains. *Antibiotics* **7**, 1–16 (2018).
45. Vianna, J. S. et al. The contribution of efflux pumps in *Mycobacterium abscessus* complex resistance to clarithromycin. *Antibiotics* **8**, 153 (2019).
46. Paixão, L. et al. Fluorometric determination of ethidium bromide efflux kinetics in *Escherichia coli*. *J. Biol. Eng.* **3**, 18 (2009).
47. Pule, C. M. et al. Efflux pump inhibitors: targeting mycobacterial efflux systems to enhance TB therapy. *J. Antimicrob. Chemother.* **71**, 17–26 (2016).
48. Koon, N., Squire, C. J. & Baker, E. N. Crystal structure of LeuA from *Mycobacterium tuberculosis*, a key enzyme in leucine biosynthesis. *Proc. Natl Acad. Sci. USA* **101**, 8295–8300 (2004).
49. Lincecum, T. L. et al. Structural and mechanistic basis of pre- and posttransfer editing by leucyl-tRNA synthetase. *Mol. Cell* **11**, 951–963 (2003).
50. Amorim Franco, T. M. & Blanchard, J. S. Bacterial branched-chain amino acid biosynthesis: structures, mechanisms, and drugability. *Biochemistry* **56**, 5849–5865 (2017).
51. de Carvalho, L. P. S., Frantom, P. A., Argyrou, A. & Blanchard, J. S. Kinetic evidence for interdomain communication in the allosteric regulation of α-isopropylmalate synthase from *Mycobacterium tuberculosis*. *Biochemistry* **48**, 1996–2004 (2009).
52. Cavalieri, D. et al. Trifluoroleucine resistance and regulation of α-isopropyl malate synthase in *Saccharomyces cerevisiae*. *Mol. Gen. Genet.* **261**, 152–160 (1999).
53. de Carvalho, L. P. S. & Blanchard, J. S. Kinetic analysis of the effects of monovalent cations and divalent metals on the activity of *Mycobacterium tuberculosis* α-isopropylmalate synthase. *Arch. Biochem. Biophys.* **451**, 141–148 (2006).
54. Eisenstein, E. Allostertic regulation of biosynthetic threonine deaminase from *Escherichia coli*: effects of isoleucine and valine on active-site ligand binding and catalysis. *Arch. Biochem. Biophys.* **316**, 311–318 (1995).
55. Lambert, R. J. W. & Pearson, J. Susceptibility testing: accurate and reproducible minimum inhibitory concentration (MIC) and non-inhibitory concentration (NIC) values. *J. Appl. Microbiol.* **88**, 784–790 (2000).
56. Bolger, A. M., Lohse, M. & Usadel, B. Trimmomatic: a flexible trimmer for Illumina sequence data. *Bioinformatics* **30**, 2114–2120 (2014).
57. Li, H. Aligning sequence reads, clone sequences and assembly contigs with BWA-MEM. Preprint at *arXiv* https://arxiv.org/abs/1303.3997 (2013).
58. Li, H. et al. The Sequence Alignment/Map format and SAMtools. *Bioinformatics* **25**, 2078–2079 (2009).
59. Garrison, E. & Marth, G. Haplotype-based variant detection from short-read sequencing. Preprint at *arXiv* https://arxiv.org/abs/1207.3907 (2012).
60. Rabodoarivelo, M. S. et al. Optimizing of a protein extraction method for *Mycobacterium tuberculosis* proteome analysis using mass spectrometry. *J. Microbiol. Methods* **131**, 144–147 (2016).
61. Waterhouse, A. et al. SWISS-MODEL: homology modelling of protein structures and complexes. *Nucleic Acids Res.* **46**, W296–W303 (2018).
62. Studer, G. et al. QMEANDisCo—distance constraints applied on model quality estimation. *Bioinformatics* **36**, 1765–1771 (2020).

ACKNOWLEDGEMENTS

We thank the entire team at the Clinical Proteomics Platform of the Research Institute of the McGill University Health Centre [RI-MUHC] for discussion and their assistance with mass spectrometry. Work in M.A.B.'s laboratory was supported by a Foundation Grant from the Canadian Institutes for Health Research (FDN-148362). J.R.S. was supported by a doctoral studentship from the Fonds de recherche du Québec. M.A.B. is the recipient of a Tier 1 Canada Research Chair. The funders played no role in the study design, data collection, analysis and interpretation of data, or the writing of this manuscript.

AUTHOR CONTRIBUTIONS

J.R.S. and M.A.B. conceived and designed experiments. J.R.S., C.C., and L.T. performed experiments. J.R.S., C.C., L.T., and O.S. analysed data. M.A.B. provided supervision and acquired funding. J.R.S. and M.A.B. wrote the manuscript with input from all authors.

COMPETING INTERESTS

The authors declare no competing interests.

ADDITIONAL INFORMATION

Supplementary information The online version contains supplementary material available at https://doi.org/10.1038/s44259-023-00005-4.

Correspondence and requests for materials should be addressed to Marcel A. Behr.

Reprints and permission information is available at http://www.nature.com/reprints

Publisher's note Springer Nature remains neutral with regard to jurisdictional claims in published maps and institutional affiliations.

Open Access This article is licensed under a Creative Commons Attribution 4.0 International License, which permits use, sharing, adaptation, distribution and reproduction in any medium or format, as long as you give appropriate credit to the original author(s) and the source, provide a link to the Creative Commons license, and indicate if changes were made. The images or other third party material in this article are included in the article's Creative Commons license, unless indicated otherwise in a credit line to the material. If material is not included in the article's Creative Commons license and your intended use is not permitted by statutory regulation or exceeds the permitted use, you will need to obtain permission directly from the copyright holder. To view a copy of this license, visit http://creativecommons.org/licenses/by/4.0/.

© The Author(s) 2023